Chapter 5

CYCLIC HOT CORROSION BEHAVIOR OF SUPER AUSTENITIC STAINLESS STEEL 904L IN AIR AT 500-650 ˚C

CHAPTER - 5

CYCLIC HOT CORROSION BEHAVIOR OF SUPER AUSTENITIC STAINLESS STEEL 904L IN AIR AT 500-650 ˚C

5.1 INTRODUCTION

In view of the increasing environment hazards, it is essential to appreciate that biomass fired plants are more environment favorable than that the fossil fuels fired plants. For a sustainable society biomass and waste are good alternatives of fossil fuels for power generation [80]. However, one negative aspect of biomass fuel is deposition of ash containing inorganic alkali chlorides and sulphates and reduction in thermal efficiency of heat exchangers and corrosion at working temperature. The usage of waste products in energy production is known as WTE (Waste to Energy). Daniel et al. [81] established phase diagrams using thermodynamic data for the $NaCl+Na_2SO_4+Na_2CO_3+KCl+K_2SO_4+K_2CO_3$ system and predicted the liquidus temperatures of the above multi-component system. The eutectic temperatures were determined for the binary systems such as $NaCl+Na_2SO_4$ (625.95 °C), $NaCl+Na_2CO_3$ (631.55 °C), $KCl+K_2SO_4$ (690.45 °C), $KCl+K_2CO_3$ (630.65 °C). Several studies have been carried out on hot corrosion of a wide range of materials such as AISI 310 steel [82], Low alloy steel [83], Cast Fe-Ni-Cr alloy [84], Fe-Ni-Cr alloys, 304L, Sanicro-28 [85], Low alloy Ferritic and Austenitic stainless steels [86, 87], 10CrMo(9-10), AISI 347 [23], with different mixtures of synthetic salts, close to compositions of biomass ash.

Studies have been carried out also on corrosion behavior of highly alloyed stainless steels from the individual salts of NaCl and KCl [23, 25, 88, 89]. KCl in the deposit is

derived from burning of biomass [90] whereas NaCl is derived from burning of municipal solid waste. Enestam et al. [23] reported that corrosivity of KCl and NaCl was similar whereas Makippa et al. [91] and Lehmusto et al. [25] reported that KCl was more corrosive than NaCl. The presence of both alkali chlorides and sulphates results in lowering of melting temperature of the deposits and accelerates the rate of corrosion. The main problematic element in biomass ash environment is potassium which combines with passivation layer of Cr_2O_3 and forms K_2CrO_4, at lower temperatures up to 400 ˚C [92]. Although, protective oxides are stable in air, they become less stable in contact with KCl at high temperature.

Considerable amount of work has been carried out on hot corrosion behavior of several super austenitic grade alloys, namely Sanicro-25& 28, SMO-254 & 654 except the 904L. It was found by Norell et al. [48] that formation of Cr-Fe spinel resisted oxidation of the 904L up to 168 h at 550 °C. However, no work has been reported on high temperature corrosion behavior of the 904L steel in such a complex salt environment. This chapter describes cyclic hot corrosion behavior of the 904L steel in synthetic biomass ash environment, using two different mixtures of $NaCl+KCl+Na_2SO_4+K_2SO_4$ salts, SM1 and SM2, with Cl:S ratio of 40:60 and 60:40 respectively, at 500-650 ˚C up to 100 h. The details of experimental procedures are given in the section 2.3 of Chapter 2.

5.2 RESULTS

5.2.1 VISUAL OBSERVATION

As described in the Chapter 2 (section 2.3.2), hot corrosion tests were performed under cyclic exposure at 500-650 ˚C for 100 h. **Figure 5.1** shows photographs of the samples hot

corroded by the SM1 and SM2 salt mixtures. The spallation of the corroded/oxidized layer can be seen clearly at the higher temperature of exposure. The corroded layer of the sample coated by SM1 was found intact following exposure at 500, 550 and 600°C whereas there was spallation from the exposure at 650 °C. On the other-hand, spallation of the corroded surface of the sample by SM2 was found to start at 550 °C and progressively increase up to 650 °C. It was observed that there was only partial melting of SM1 from the exposure of 100 h at 500 °C whereas there was uniform melting of the SM2. Tiny spots of creamy color may be observed all over the surface of the samples exposed at 550-600 °C for 100 h. On the other hand, there are pale yellow spots on the surface of the SM2 coated sample and spallation of the scale from the flat surface as well as exfoliation along the periphery. However, there was no spallation due to SM1 coating; a few spots of salt remnants were observed after 100 h of exposure. The yellow spots may be due to salt reactions with surface oxides and formation of potassium/sodium chromates.

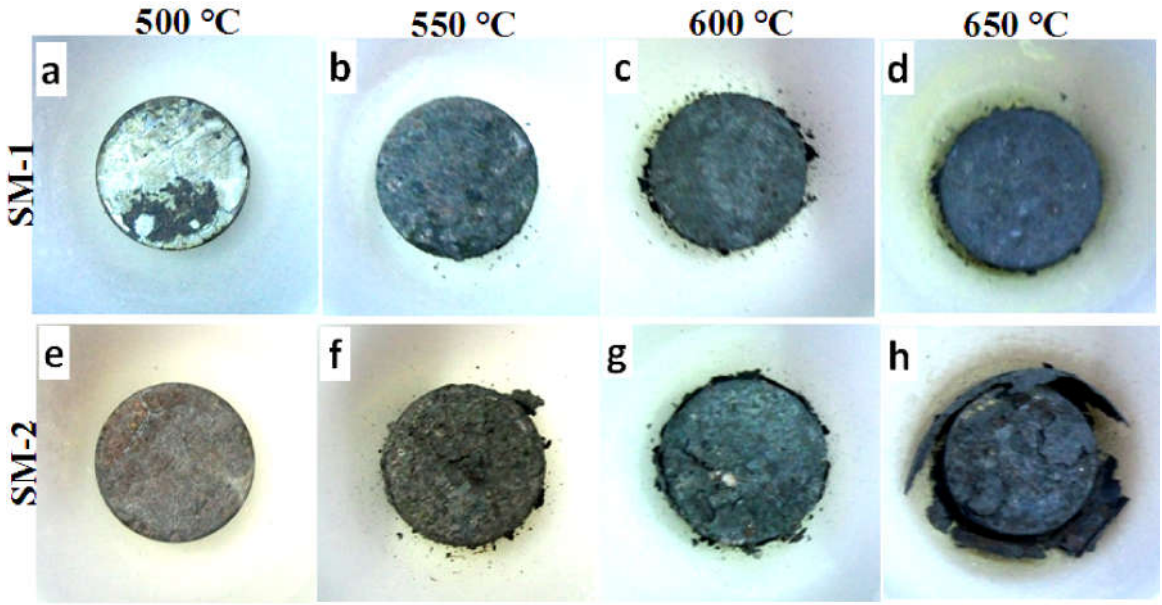

Figure 5.1: Photographs of the samples corroded at 500-650 °C for 100 h by: (a,b,c,d) SM1 and (e,f,g,h) SM2.

5.2.2 WEIGHT GAIN ANALYSIS

Figure 5.2a and **5.2b** show plots of weight change per unit area (mg/cm^2) (ΔW) versus time interval of 15 cycles for the samples, coated with SM1 and SM2 respectively, exposed in air atmosphere at 500, 550, 600 and 650 ˚C for 100 h. It is evident that there is much higher weight gain in the samples coated with the SM2 coating than in those coated with SM1. Thus, it is obvious that there was more rapid formation of oxides and other corrosion products from the coating of SM2. The inserts in the plots show that weight gain during the initial period of 5 h was much less than that beyond 5 h of exposure, in the samples coated with both SM1 as well as SM2. However, the weight gain even during the initial stage of 5 h is relatively higher from SM2 than from the SM1 coating. **Figure 5.3(a-b)** shows the variation of square of weight gain per unit area $(\Delta W)^2$ with duration of exposure up to 100 h. There is rapid increase in $(\Delta W)^2$ during the exposure of 5-25 h at 600 ºC and significantly more at 650 °C in the sample coated with SM2, thereafter the increase is much slower during 25-100 h of exposure, and a dual slope behavior is exhibited (**Figure 3b**).

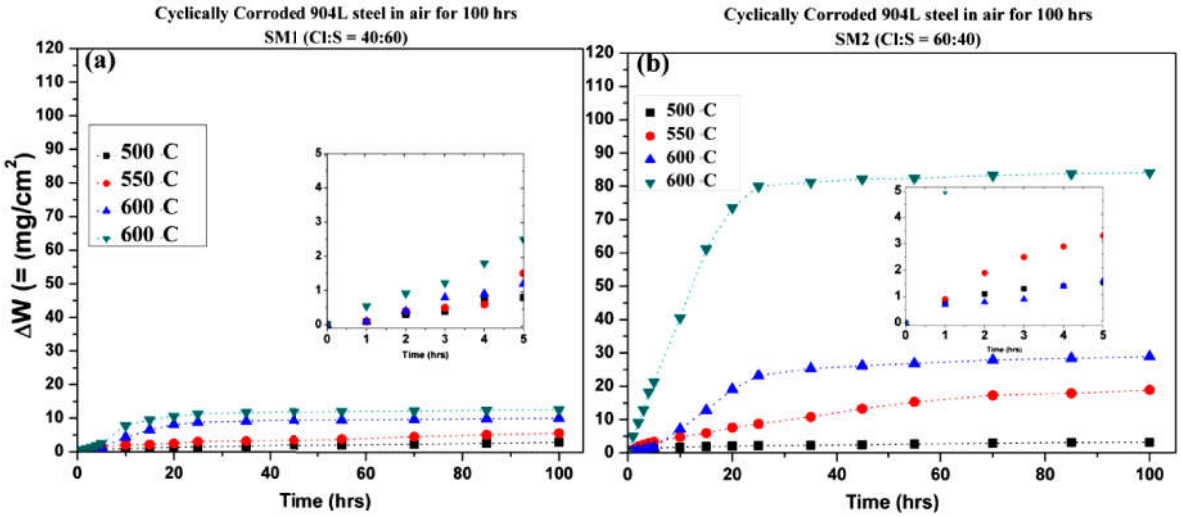

Figure 5.2: Weight change per unit area (ΔW) versus time plots of the samples exposed at 500-650 ˚C up to 100 h and corroded from: (a) SM1(Cl:S=40:60) and (b) SM2(Cl:S=60:40).

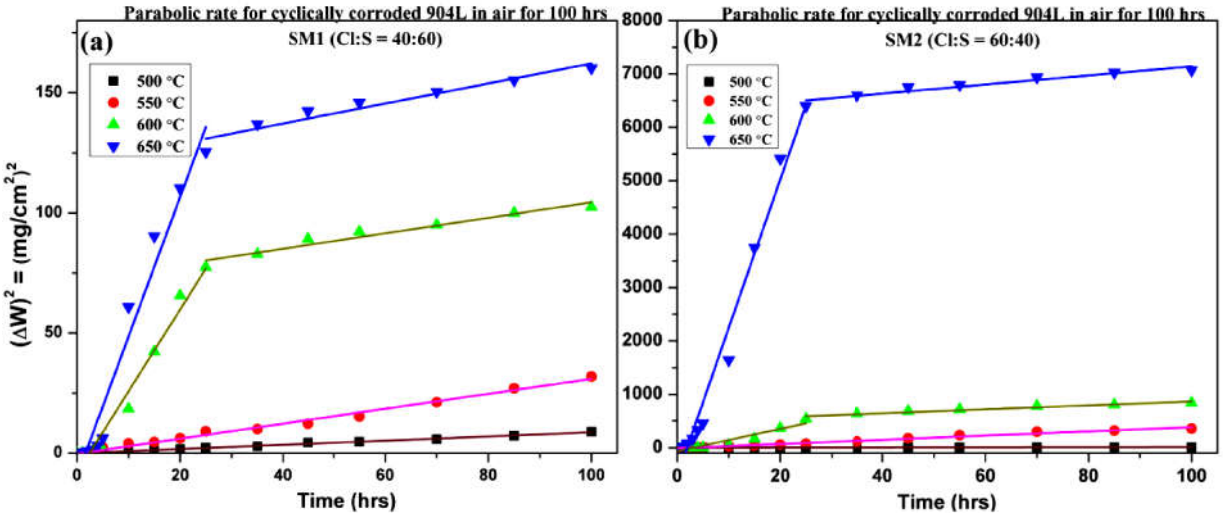

Figure 5.3: Square of weight gain per unit $(\Delta W)^2$ versus time plots of the samples exposed at 500-650 ˚C up to 100 h and corroded from: (a) SM1(Cl:S=40:60) coated and (b) SM2(Cl:S=60:40) coated.

On the other hand there is relatively much less increase in $(\Delta W)^2$ from the exposure at 500 and 550 ºC and the increase is linear with a single slope during the exposure from 5-100 h. The variation of $(\Delta W)^2$ with the duration of exposure in the sample coated with SM1 (**Figure 5.3a**) is similar to that coated with SM2 (**Figure 5.3b**), however, the increase from SM1 is much less than that from SM2, as the scale of $(\Delta W)^2$ in **Figure 5.3b** is much higher than that in **Figure 5.3a**. The corrosion kinetics may be seen to follow parabolic rate law $\Delta W^2 = k_p t + c$, where ΔW is weight gain per unit area, t is the exposure time, k_p is rate constant and c is a constant. The estimated values of kp are presented in **Table 5.1** which are much higher for the samples coated with SM2 than those coated with SM1, above 500 ºC. It is also evident that kp values at 600 and 650 ºC are much higher corresponding to 5-25 h of exposure than those for 25-100 h of exposure.

Table 5.1: Parabolic rate constants for the samples hot corroded with SM1 and SM2 salt mixtures from 500-650 °C, up to 100 h.

	SM1 (Cl:S = 40:60)				***SM2 (Cl:S = 60:40)***			
Temperature. (˚C)	**ΔW (mg)**	**Time (h)**	**k_p**	**R^2**	**ΔW (mg)**	**Time (h)**	**k_p**	**R^2**
500	2.9	0-100	0.09	0.99	3.1	0-100	0.09	0.94
550	5.7	0-100	0.31	0.99	18.9	0-100	3.92	0.98
600	8.8	0-25	3.4	0.96	23.2	0-25	20.79	0.90
	10.1	25-100	0.32	0.94	28.9	25-100	3.68	0.91
650	11.2	0-25	5.81	0.96	80	0-25	278.4	0.98
	12.66	25-100	0.42	0.92	84.1	25-100	8.51	0.91

Note: Unit for k_p is $(mg^2 \cdot cm^{-4} \cdot h^{-1})$

5.2.3 XRD ANALYSIS

XRD patterns of the samples with SM1 and SM2 coatings exposed in air from 500-650 ºC are shown in **Figure 5.4a and 5.4b** respectively. Details of the analysed peaks are presented in **Table 5.2**. XRD peaks of the samples exposed at 500 ˚C do not correspond to any strong phase other than chromium and iron combined with chlorides and sulphates.

Spinels of Cr-Ni-Fe and Cr-Mn-Cu oxides are observed along with the corrosives FeS, $FeCl_3$ and CrS in the samples coated with SM1 and $K_2Cr_2O_7$ and K_2FeO_4 in those coated with SM2. At 550 ºC similar features are observed with formation of spinels of transition elements oxides. Corrosion products namely $KCrO_2$ and $NaCrO_2$ are evolved with SM1 salt mixture whereas $NaFeO_2$ and $Na_2Cr_2O_7$ are formed with SM2. At 600 ºC corrosion from the salt mixture resulted in formation of a new phase Cr_2MnO_4 in both the samples coated with SM1 as well as SM2. Also, there is extensive formation of Na-K-Fe-Cr-O based corrosion products along with Fe-Cr-S-Cl system. At 650 ºC, there was formation of K_2CrO_4 and Na_2CrO_4, new phases of corrosion products. **Table 5.3** shows the various corrosion and oxidation reactions at different temperatures of exposure.

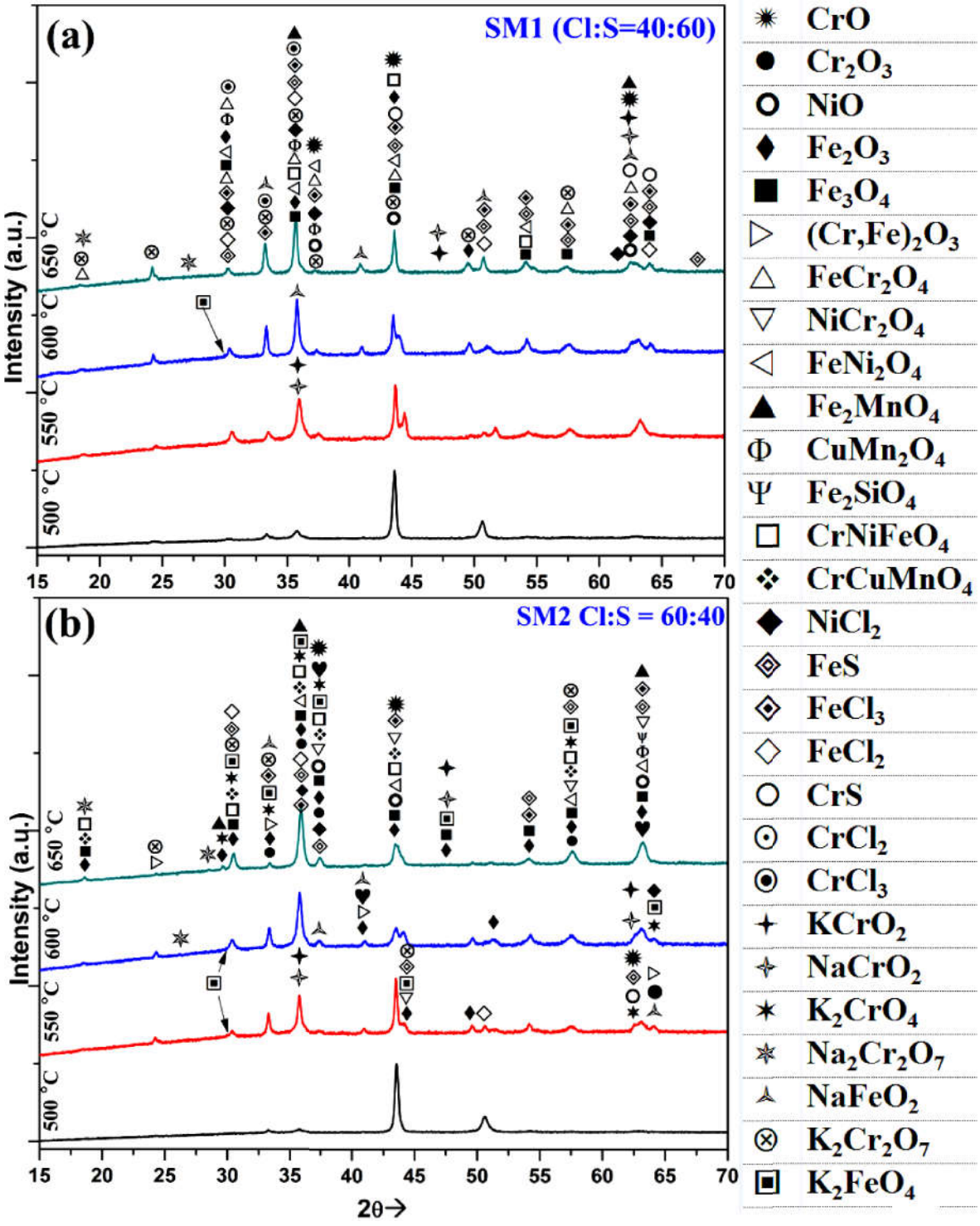

Figure 5.4: Phase analysis of the corrosion products by XRD, resulting from exposure at 500-650 ˚C up to 100 h and corroded by: (a) SM1 and (b) SM2.

Table 5.2: Various phases and compounds formed from hot corrosion of 904L steel by SM1 and SM2 salt mixtures, exposed from 500 to 650 ° C, up to 100 h.

	SM1 (Cl:S=40:60)		SM2 (Cl:S=60:40)	
Temperature	**Oxides Products**	**Corrosive Products**	**Oxides Products**	**Corrosive products**
500 °C	CrO, Cr_2O_3, Fe_2O_3, Fe_3O_4, NiO, Cr_2NiO_4, $FeNi_2O_4$, Cr_2FeO_4, $CuMn_2O_4$, $CrFeNiO_4$, $CrCuMnO_4$, Fe_2MnO_4, Fe_2SiO_4, $(Fe,Cr)_2O_3$	FeS, $FeCl_3$, CrS,	CrO,Cr2O3, Fe_2O_3, Fe_3O_4, NiO, Cr_2NiO_4, $FeNi_2O_4$, Cr_2FeO_4, $CuMn_2O_4$, $CrFeNiO_4$, $CrCuMnO_4$, Fe_2MnO_4, Fe_2SiO_4, $(Fe,Cr)_2O_3$	FeS, $FeCl_3$, CrS, $K_2Cr_2O_7$, K_2FeO_4,
550 °C	CrO, Cr_2O_3, Fe_2O_3, Fe_3O_4, NiO, Cr_2NiO_4, $FeNi_2O_4$, Cr_2FeO_4, $CuMn_2O_4$, $CrFeNiO_4$, $CrCuMnO_4$, Fe_2MnO_4, Fe_2SiO_4, $(Fe,Cr)_2O_3$	FeS, $FeCl_3$, CrS, $NiCl_2$, K_2FeO_4, $KCrO_2$, $NaCrO_2$,	CrO, Cr_2O_3, Fe_2O_3, Fe_3O_4, NiO, Cr_2NiO_4, $FeNi_2O_4$, Cr_2FeO_4, $CuMn_2O_4$, $CrFeNiO_4$, $CrCuMnO_4$, Fe_2MnO_4, Fe2SiO4, $(Fe,Cr)_2O_3$	FeS, $FeCl_3$, CrS, $K_2Cr_2O_7$, $NiCl_2$, K_2FeO_4, $KCrO_2$, $NaCrO_2$, $Na_2Cr_2O_7$, $NaFeO_2$
600 °C	CrO,Cr_2O_3, Fe_2O_3, Fe_3O_4, NiO, Cr_2NiO_4, $FeNi_2O_4$, Cr_2FeO_4, $CuMn_2O_4$, Cr_2MnO_4, $CrFeNiO_4$, $CrCuMnO_4$, Fe_2MnO_4, Fe_2SiO_4, $(Fe,Cr)_2O_3$	FeS, FeCl3, CrS, $NiCl_2$, $K_2Cr_2O_7$, K_2FeO_4, $KCrO_2$, $NaCrO_2$, $Na_2Cr_2O_7$, $NaFeO_2$	CrO,Cr_2O_3, Fe_2O_3, Fe_3O_4, NiO, Cr_2NiO_4, $FeNi_2O_4$, Cr_2FeO_4, $CuMn_2O_4$, Cr_2MnO_4, $CrFeNiO_4$, $CrCuMnO_4$, Fe_2MnO_4, Fe_2SiO_4, $(Fe,Cr)_2O_3$	FeS, $FeCl_3$, CrS, $K_2Cr_2O_7$, $NiCl_2$, K_2FeO_4, $KCrO_2$, $NaCrO_2$, $Na_2Cr_2O_7$, $NaFeO_2$
650 °C	CrO,Cr_2O_3, Fe_2O_3, Fe_3O_4, NiO, Cr_2NiO_4, $FeNi_2O_4$, Cr_2FeO_4, $CuMn_2O_4$, Cr_2MnO_4, $CrFeNiO_4$,$CrCuMnO_4$, Fe_2MnO_4, Fe_2SiO_4, $(Fe,Cr)_2O_3$	FeS, $FeCl_3$, CrS, $NiCl_2$, $K_2Cr_2O_7$, K_2FeO_4, $KCrO_2$, $NaCrO_2$, $Na_2Cr_2O_7$, $NaFeO_2$,	CrO,Cr_2O_3, Fe_2O_3, Fe_3O_4, NiO, Cr_2NiO_4, $FeNi_2O_4$, Cr_2FeO_4, $CuMn_2O_4$, Cr_2MnO_4, $CrFeNiO_4$, $CrCuMnO_4$, Fe_2MnO_4, Fe_2SiO_4, $(Fe,Cr)_2O_3$	FeS, $FeCl_3$, CrS, K_2CrO_4, $NiCl_2$, K_2FeO_4, $KCrO_2$, $NaCrO_2$, Na_2CrO_4

5.2.4 SURFACE MORPHOLOGY

The relative inhomogeneities of the surface morphology and development of scales on the samples in respect to the Cl:S ratio in the two salt mixtures were analysed by SEM-EDS.

The micrographs in **Figures 5.5a, 5.6a, 5.7a** and **5.8(a-b)** show top surfaces of the samples corroded by SM1 and those in Figures 5.5b, 5.6b, 5.7b and 5.9(a-b) show surface morphology of the samples corroded by SM2, from 100 h of exposures at 500-650 ˚C. At

all the temperatures of the exposure, coating of the both SM1 and SM2 resulted in characteristic morphology of metals oxides and corrosion products over the surface. The scale formed from SM1 was intact and there was no spallation (**Figure 5.5a**) whereas the coating of SM2 had cracked at some places and also spalled (**Figure 5.5b**).

Figure 5.5a and **5.5b** show the samples corroded with SM1 and SM2 respectively, from the exposure at 500 °C for 100 h, exhibiting less oxidation/corrosion.

Table 5.3: Possible oxidation/corrosion reactions and their products formed from hot corrosion of 904L steel by SM1 and SM2 from 500 °C to 650 °C.

No.	Reactant	=	Product
1	$Cr(s) + 0.5O_2(g)$	=	$CrO(s)$
2	$2CrO(s) + 0.5O_2(g)$	=	$Cr_2O_3(s)$
3	$Cr(s) + Cl_2(g)$	=	$CrCl_2(s)$
4	$CrCl_2(s) + 0.5Cl2(g)$	=	$CrCl_3(s)$
5	$Cr(s) + 1.5Cl_2(g)$	=	$CrCl_3(s)$
6	$Cr(s) + SO_4^{(-2)}(g)$	=	$CrS(s) + 2O_2^{(-2)}(g)$
7	$2KCl(s) + Cr_2O_3(s) + O_2(g)$	=	$K_2CrO_4(s) + CrO(s) + Cl_2(g)$
8	$2KCl(s) + 2CrO(s) + O_2(g)$	=	$K_2CrO_4(s) + Cl_2(g)$
9	$2KCl(s) + Cr_2O_3(s) + 2O_2(g)$	=	$K_2Cr_2O_7(s) + Cl_2(g)$
10	$2KCl(s) + Fe_3O_4 + 1.5O_2(g)$	=	$K_2FeO_4(s) + Fe_2O_3(s) + Cl_2(g)$
11	$2KCl(s) + Fe_2O_3 + 0.5O_2(g)$	=	$K_2FeO_4 + FeCl_2$
12	$2CrCl_2(s) + 1.5O_2(g)$	=	$Cr_2O_3(s) + 2Cl_2(g)$
13	$2CrCl_3(s) + 1.5O_2(g)$	=	$Cr_2O_3(s) + 3Cl_2(g)$
14	$FeCl_2(g) + 2O_2(g)$	=	$Fe_3O_4(s) + 3Cl_2$
15	$FeCl_2(g) + 1.5O_2(g)$	=	$Fe_2O_3(s) + 2Cl_2(g)$
16	$NiCl_2(g) + 0.5O_2(g)$	=	$NiO(s) + Cl_2(g)$
17	$NiO(s) + Cr_2O_3(s)$	=	$NiCr_2O_4(s)$
18	$NiO(s) + Fe_2O_3(s)$	=	$NiFe_2O_4(s)$
19	$NiO(s) + 0.5Fe_2O_3(s) + 1.5O_2(g)$	=	$Ni_2FeO_4(s)$
20	$2FeO(s) + 2Cr_2O_3(s) + 1.5O_2(g)$	=	$2FeCr_2O_4(s)$
21	$Na_2O + Cr_2O_3(s) + 1.5O_2(g)$	=	$Na_2Cr_2O_7(s)$
22	$MnO(s) + Fe_2O_3(s)$	=	$MnFe_2O_4(s)$
23	$MnO(s) + Cr_2O_3(s)$	=	$MnCr_2O_4(s)$
24	$2NaCl(s) + Fe_2O_3(s) + 0.5O_2(g)$	=	$Na_2Fe_2O_4(s) + Cl_2(g)$
25	$4NaCl(s) + Cr_2O_3(s) + 2.5O_2(g)$	=	$2Na_2CrO_4(s) + 2Cl_2(g)$
26	$FeCl_2(s)$	=	$FeCl_2(g)$
27	$Fe_2O_3(s) + 2(Na,K)Cl + 0.5O_2(g)$	=	$(Na,K)_2Fe_2O_4(s) + Cl_2(g)$
28	$Cr_2O_3(s) + 2(Na,K)Cl(s) + 2O_2(g)$	=	$(Na,K)_2Cr_2O_7(s) + Cl_2(g)$
29	$2(Na,K)Cl(s) + Cr_2O_3(s) + 0.5O_2(g)$	=	$2(Na,K)CrO_2(s) + Cl_2(g)$
30	$K_2O(s) + FeO(s) + O_2(g)$	=	$K_2FeO_4(s)$
31	$2NaCl(s) + Fe_2O_3(s) + 0.5O_2(g)$	=	$2NaFeO_2(s) + Cl_2(g)$

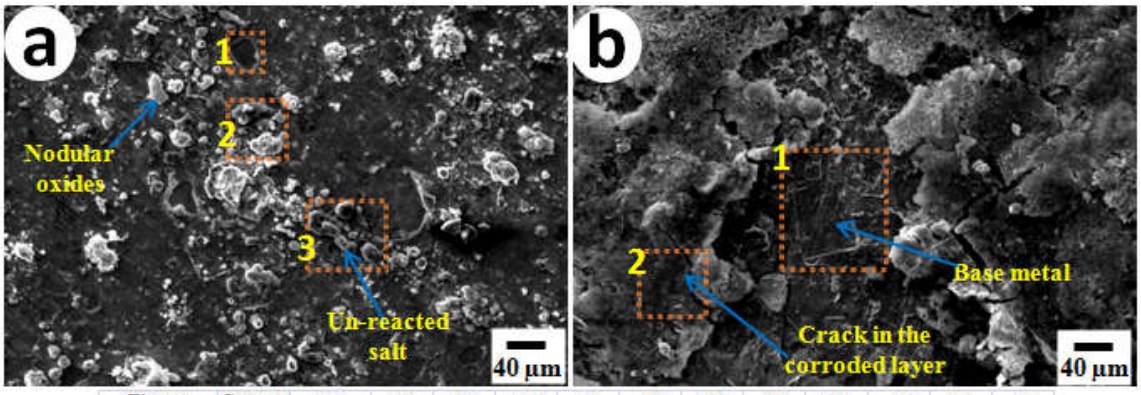

Figure	Spectru	Mn	Mo	Cr	Ni	Fe	Si	Cu	O	Na	K	S	Cl
At 500 °C SM1	1	1.57	3.39	17.2	29	36.4	0.21	0.97	8.88	1.04	0.32	0.93	0.08
	2	0.64		5.8	44	20.9		0.36	21.6	0.41		0.93	5.31
	3	2.42	1.01	10.3	9	42.6	0.58	1.03	30.8	1.72	0.2		0.34
	FULL	1.11	1.56	15.3	19.5	36.2	0.15	1.04	22.5	0.61	0.18	1	0.91
At 500 °C SM2	1	0.36	6.62	20.6	15.5	22.5	0.61	0.03	29.7		0.14	3.04	0.92
	2	0.13		3.4	19.5	25.3	0.21	1.25	44.7		0.27	3.97	1.18
	FULL	2.05		11.4	11.6	41.1	0.22	1.68	27.5	1.44	0.42	1.82	0.69

Figure 5.5: Surface morphology of the samples exposed up to 100 h at 500 ºC and corroded by: (a) SM1 and (b) SM2.

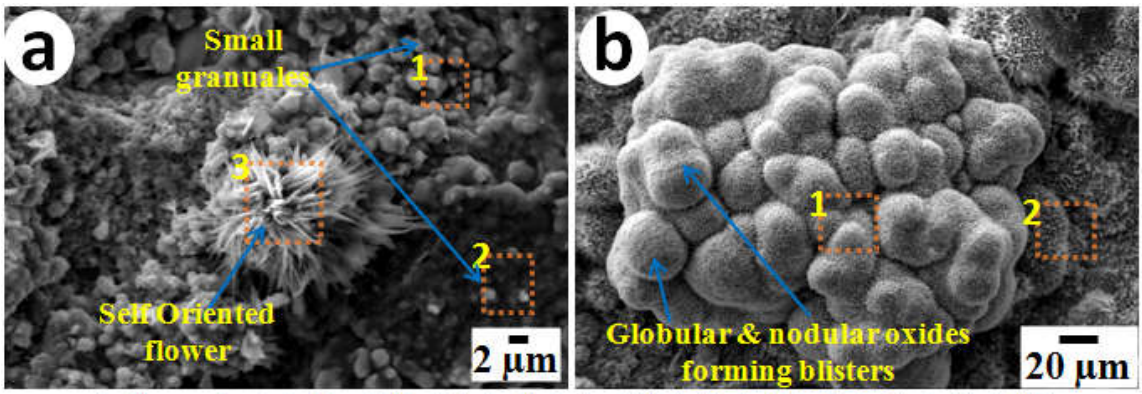

Figure	Spectrum	Mn	Mo	Cr	Ni	Fe	Si	Cu	O	Na	K	S	Cl
At 550 °C SM1	1	4.88		3.15		62.6		5.29	23.5		0.62		
	2	12.95		5.85	5.99	37.1			30.9	2.94	2.4	1.87	
	3			12.70	13.44	38.69			29.21	2.36	1.13	1.10	1.37
At 550 °C SM2	1	2.98	1.7	0.82	13.1	25.9	0.32	1.86	37.9	7.87	4.29	2.05	1.27
	2	0.87	2.49	21.02	21.62	8.47	0.02	0.62	28.72	12.02	1.12	0.27	2.76

Figure 5.6: Surface morphology of the samples exposed up to 100 h at 550 ºC and corroded by: (a) SM1 and (b) SM2.

In **Figure 5.6a**, the surface of the sample corroded by SM1 at 550 °C shows small granules of oxide particles, uniformly grown all over the surface. The morphology of the product formed with SM1 at 550 °C shows self-oriented flowers and features like cactus needle, grown in between the oxide granules whereas the sample corroded by SM2 shows oxide morphology of globular/nodular shape (**Figure 5.6b**). This morphology is like a cauliflower and there are globular domes. This type of morphology can be understood from localized blistering of the scale by volatile products and pushing of scale outward [17].

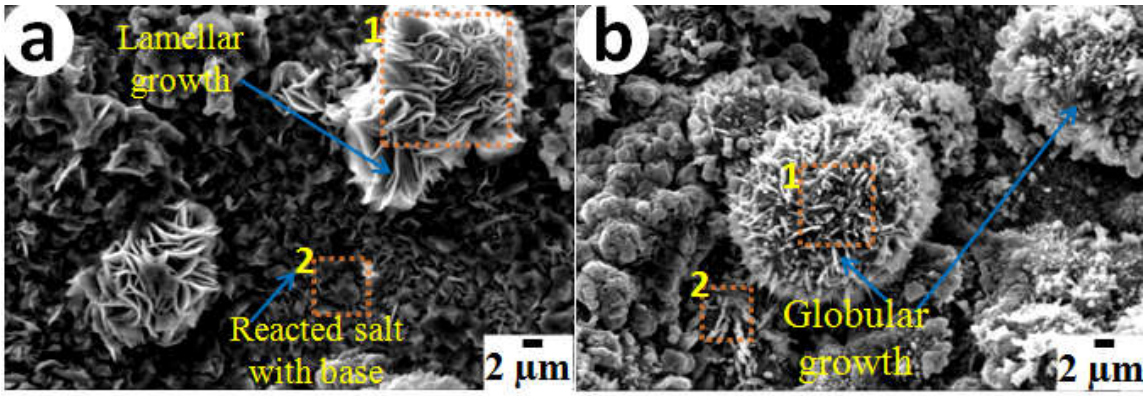

Figure	Spectrum	Mn	Mo	Cr	Ni	Fe	Si	Cu	O	Na	K	S	Cl
At 600 °C	1	3.6	0.09	11.5	9.65	38.2	0.32	0.01	35.1	0.98	0.62		
SM1	2	1.86	0.6	16.9	9.67	44.3		0.04	20.1	2.4	3.2	0.19	0.78
At 600 °C	1		2.65	7.52	42.76	19.69		2.95	24.43				
SM2	2	2.65	1.01	9.72	26.46	30.03		3.10	26.85		0.19		

Figure 5.7: Surface morphology of the samples exposed up to 100 h at 600 ºC, corroded by (a) SM1 and (b) SM2.

The morphology of the surface resulting from corrosion at 600 °C due to SM1 and SM2 salt mixtures may be seen in **Figure 5.7a and 5.7b** respectively. It is clear that from SM1 there was formation of globular nodules and also spallation of the scale. The magnified image shows lamellar structure, with higher content of Fe-Ni-Cr spinel, as revealed by EDS analysis. As shown in **Figure 5.7b**, there was spallation of the sample coated with SM2 and exposed at 600 °C. In this condition, from 550 to 600 °C, oxides are

almost similar but differ in morphology. Oxide nodules may be seen to be irregular in shape (**Figure 5.7b**).

Figure 5.8a shows the morphology of the layer lying beneath the spalled layer of the sample coated with SM1 and exposed at 650 °C. Oxides granules are uniformly distributed all over the surface beneath the spalled layer. **Figure 5.8b** shows morphology of the scale which did not spall. The unspalled layer shows nodular/irregular shape of oxide nodules of Cr-Ni spinels.

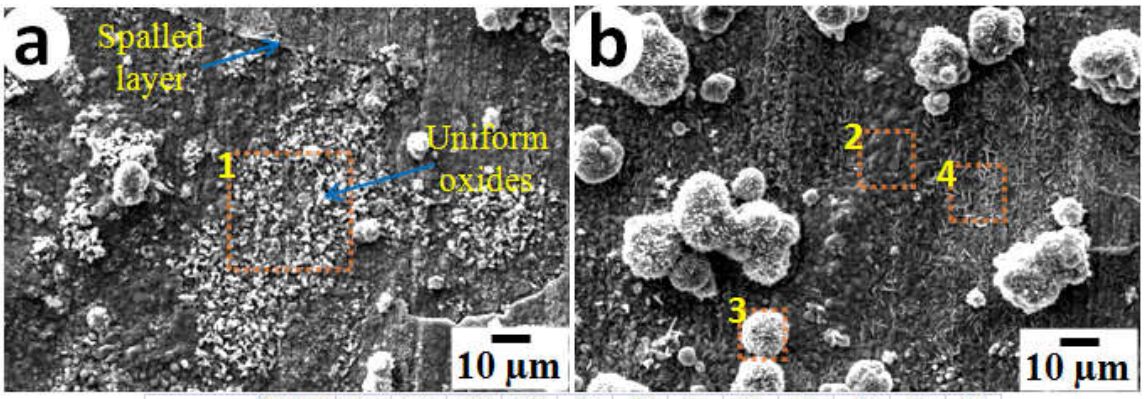

	Spectrum	Mn	Mo	Cr	Ni	Fe	Si	Cu	O	Na	K	S	Cl
At 650 °C SM1	1	2.53	0.06	13.7	1.6	54.2	0.24		28.6			0.09	
	2	3.63		8.03	2.69	55.4		1.57	28.6	0.01			0.04
	3	2.85		6.94	0.7	60.6		1.94	26.8				0.21
	4	4.52		7.58	3.07	51.4	0.27	1.8	30.7	0.22	0.11	0.31	0.07

Figure 5.8: Surface morphology of the samples coated with SM1 and exposed at 650 ºC up to 100 h showing: (a) spallation and (b) no spallation.

Figure 5.9a shows formation of dense filament like feature of Ni-Cr-Fe spinel in the region without spallation. Further, at 650 °C there is formation of two types of regions: one with filament like features and the other without such features. **Figure 5.9b** shows the region where spalled layer is not present and the region beneath the spalled layer, with cuboidal shaped Fe-Ni spinels.

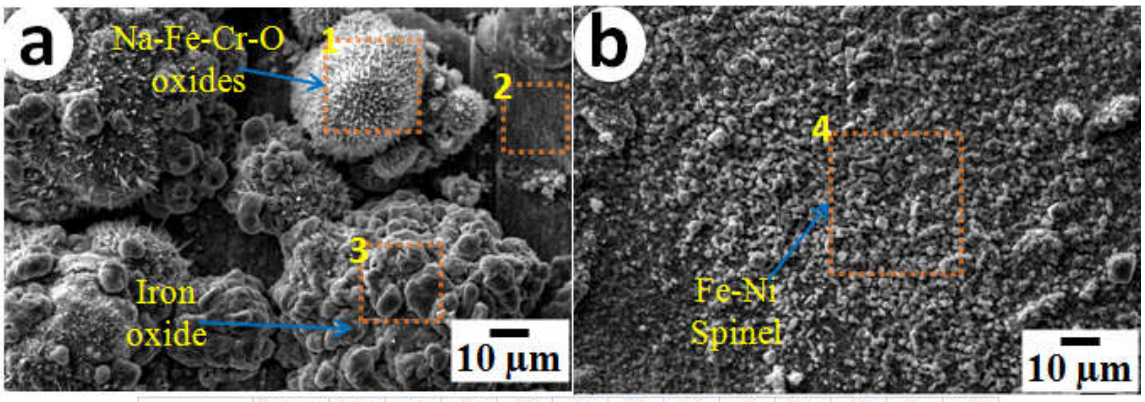

	Spectrum	Mn	Mo	Cr	Ni	Fe	Si	Cu	O	Na	K	S	Cl
At 650 °C SM2	1	2.43		9.67	0.68	47.2		0.83	38	0.93		0.03	0.16
	2	2.04	3.71	11	30.2	25.2	0.81	0.62	25.5		0.44	0.37	0.11
	3	2.73		5.65	1.96	61.8	0.03	1.38	26.1			0.22	0.15
	4	2.49	1.11	7.07	17.2	40.6	0.24	3.92	26.6	0.1		0.24	0.35

Figure 5.9: Surface morphology of the sample coated with SM2 and exposed at 650 ºC, up to 100 h showing: (a) no spallation and (b) region below the spalled scale.

5.2.5 SEM CROSS SECTIONAL ANALYSIS

Cross sections of the corroded samples were analysed by SEM-EDS and EPMA.

Figure 5.10a and 5.10b show SEM-micrographs of cross sections of the samples corroded by SM1, exposed at 500 and 550 °C whereas **Figure 5.10c** and **5.10d** show the features corroded by SM1 at 600 and 650 °C respectively. The intact layer of the oxide in **Figure 5.10a** reveals negligible corrosion and absence of internal corrosion. From the EDS analysis it was found that there was no depletion of elements with increment in temperature from 550 to 600 °C, however, there was internal attack as well as depletion and cracking along and also beneath the scale. This internal corrosion appears to be higher at 600 °C than that at 550 °C where the scale interface is intact to the base material. From the EDS analysis over the cross section in **Figure 5.10c** and **5.10d**, it was observed that there was higher depletion of Fe-Cr.

Figure 5.11a and **5.11b** show SEM-micrographs of cross sections of the samples corroded at 500 and 550 °C by SM2. It may be seen that there was greater attack from the SM2 as compared with that from SM1. SEM micrographs of the samples corroded at 600 and 650 °C are shown in **Figure 5.11c** and **5.11d** respectively, where it may be observed that severe corrosion had occurred due to SM2 and there was porous region beneath the scale interface. The corrodents locally attacked the base metal through the porous scale. This region may be presented as a layer of porous γ-Fe_2O_3/Fe_3O_4, and the internal part of the depleted zone is in the form of chromium oxide with the other constituents and showed high amount of chromium by EDS analysis. The depth of the corroded layer was ≈16-18 μm in the sample coated with SM1 and ≈31-33 μm coated with SM2.

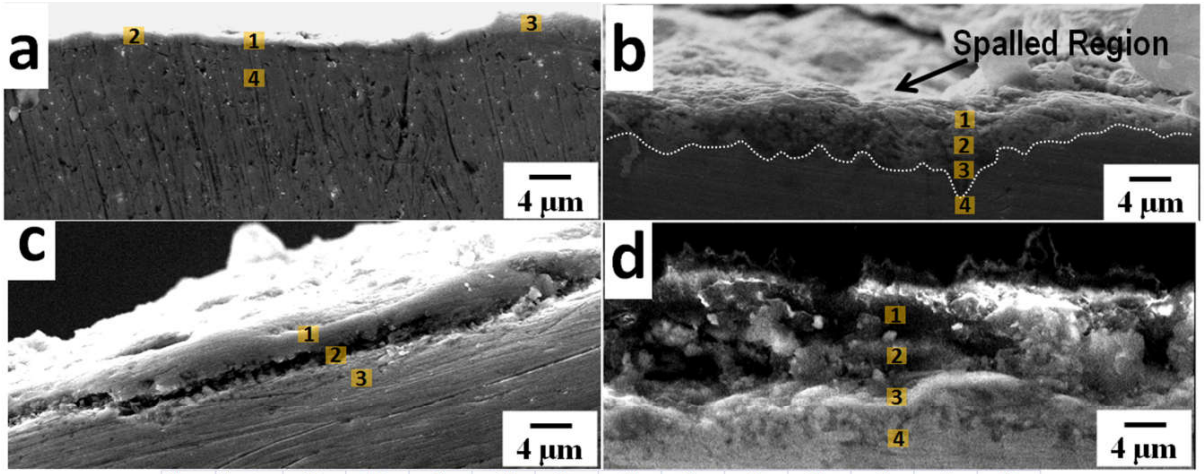

Figure	Spectrum	Mn	Mo	Cr	Ni	Fe	Si	Cu	O	Na	K	S	Cl
5.10a	1	1.15	1.56	22.02	22.52	43.33	0.21		7.05		0.54	1.63	
	2	1.06	3.26	19.72	24.39	48.49	0.22	2.05	0.63	0.00	0.00	0.08	0.11
	3	0.80	4.11	18.77	22.65	48.33	0.41	1.81	1.50	1.07	0.11	0.27	0.15
	4	0.31	1.87	20.02	23.10	50.46	0.23	1.70	0.63		0.28	1.39	0.01
5.10b	1	0.89	1.75	11.94	45.05	26.84	1.20	1.31	8.71	1.15	0.16	1.01	
	2	0.02	5.10	3.03	73.12	10.34	0.65		6.53		0.04	0.72	0.45
	3	0.66	2.98	11.29	48.68	31.04	0.27	0.15	2.85			2.09	11.29
	4	1.43	2.85	23.37	23.50	45.76	1.60	0.56				0.62	0.40
5.10c	1	1.54	3.59	18.28	20.25	41.66	3.19	0.29	9.62	1.45			1.14
	2	2.18	5.67	14.76	19.49	30.19	2.66	1.22	21.87	1.00	0.41		0.55
	3	0.47	2.14	12.60	39.36	33.88	3.02		6.13			2.30	0.10
5.10d	1	1.25	2.99	20.68	26.40	44.89		1.98	0.64	0.09	0.10		0.97
	2	2.26	5.53	19.15	23.16	44.54	0.11		4.78				0.48
	3	1.33	2.74	20.12	22.32	47.77	0.22	1.73	1.50	0.72	0.12	1.15	0.29
	4	3.00	4.28	20.01	22.54	45.86	0.62	0.36	2.78		0.26	0.23	0.05

Figure 5.10: SEM micrographs showing cross sectional features of the samples hot corroded by SM1 up to 100 h at: (a) 500, (b) 550, (c) 600 and (d) 650 °C; up to 100 h.

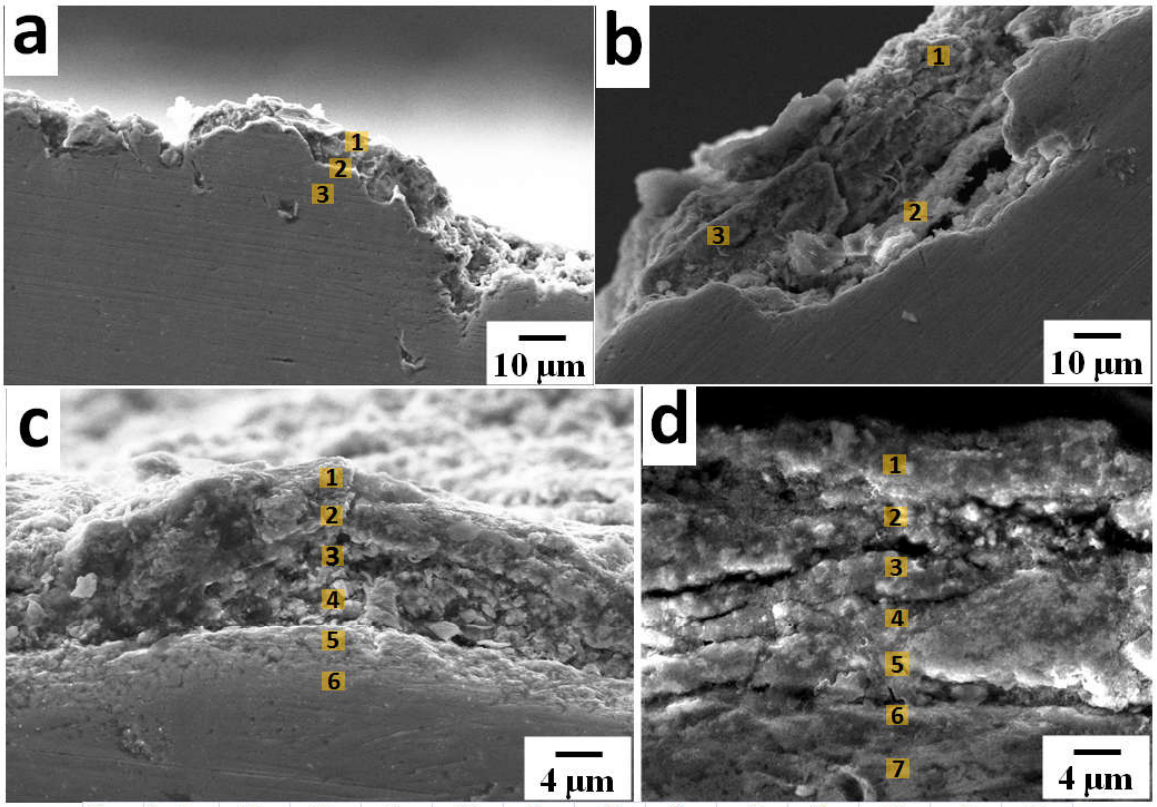

Figure	Spectrum	Mn	Mo	Cr	Ni	Fe	Si	Cu	O	Na	K	S	Cl
5.11a	1	1.12	3.4	22.46	20.61	43.38	0.43	1.39	6.11	0.23	0.3	0.39	0.18
	2	2.4	0.28	18.52	24.56	44.27	0.08	1.89	4.61	2.32		0.84	0.11
	3		3.34	21.2	24.73	49.09	0.37	1.03	0.24				
5.11b	1	0.55		23.47	7.54	21.2	0.9		43.24		1.14	1.96	
	2	2.15	2.27	19.53	20.84	38.68	0.92	1.31	13.21		0.25		0.84
	3	2.38		16.97	20.82	33.83	0.04		23.04		1.18	0.74	1.01
5.11c	1	2.27	0.64	9.88	29.69	37.47	4.07	0.17	14.52	0.46	0.70	0.13	
	2	0.73		13.43	20.38	22.03	1.59	1.31	36.93	1.51	0.47	1.16	0.46
	3	0.38		17.06	23.48	52.51	2.43	1.01	2.34		0.39		0.40
	4	3.44	3.10	11.46	45.25	28.03	0.44		6.42			1.26	0.62
	5	1.44	6.62	14.59	40.88	26.84	1.67	1.34	5.97	0.06		0.05	0.57
5.11d	1	0.25		2.62	5.1	57.78	0.72	0.53	32.64		0.37		
	2	2.73	3.66	22.31	22.32	45.68		0.33	1.99		0.18	0.04	0.78
	3	0.15	1.59	19.1	17.59	27.47	0.42		32.75		0.49	0.44	
	4	1.89		29.79	21.57	39.59	0.39	2.99	3.36		0.42		
	5		0.02	6.6	65.28	24.75			0.28	1.34	0.28	1.44	
	6	0.72	4.34	18.33	23.14	43.19	0.66	1.95	7.68				
	7	1.49	2.89	18.92	22.11	46.48			7.36			0.55	0.21

Figure 5.11: SEM micrographs showing cross section of the samples hot corroded by SM2 up to 100 h at: (a) 500, (b) 550, (c) 600 and (d) 650 °C.

5.2.6 EPMA ANAYLSIS

Figures 5.12(a-b) and 5.13(a-b) show EPMA analysis of cross sections of the samples corroded with SM1 and SM2 at 650 °C for 100 h. The severity of corrosion from SM2 with 60:40 (Cl:S) ratio is quite evident and there is also internal attack. A scale of layers, with a thick depleted region can be seen between the internal scale at the substrate and the outer scale on the surface of the sample with SM2 coat, as compared with the much thinner scale resulting from SM1. Moreover, after 100 h of exposure, it can be seen from **Figure 5.12a** that the layer formed from SM1 constituted of dual phase layer. **Figure 5.12b** shows distribution maps of different elements (Cr, Ni, Fe, Mn, Mo and O). In case of the sample with SM2, multiphase layer can be seen in **Figure 5.13(a-b)**. From the color contrast in the EPMA maps in **Figure 5.13b**, the distribution of respective elements in the scale and the substrate may clearly be seen. The relative width of the scale and the depletion zone in the samples coated with SM1 and SM2 can be seen in the **Figure 5.14a and 5.14b** respectively along with concentration of the elements in these zones. According to line scan analysis, in **Figure 5.14a** the scale consists of iron and oxygen and the depletion zone constitutes of Cr-Fe-O as well as some amount of Ni close to the base metal. On the other hand **Figure 5.14b** shows that the scale resulting from SM2 is much wider and consists of Fe, Cr and O and the large depletion zone shows presence of Cr, Ni, Fe and O. The details of the depth of attack from the surface in the scale and the depletion zone is summarized in **Table 5.4**.

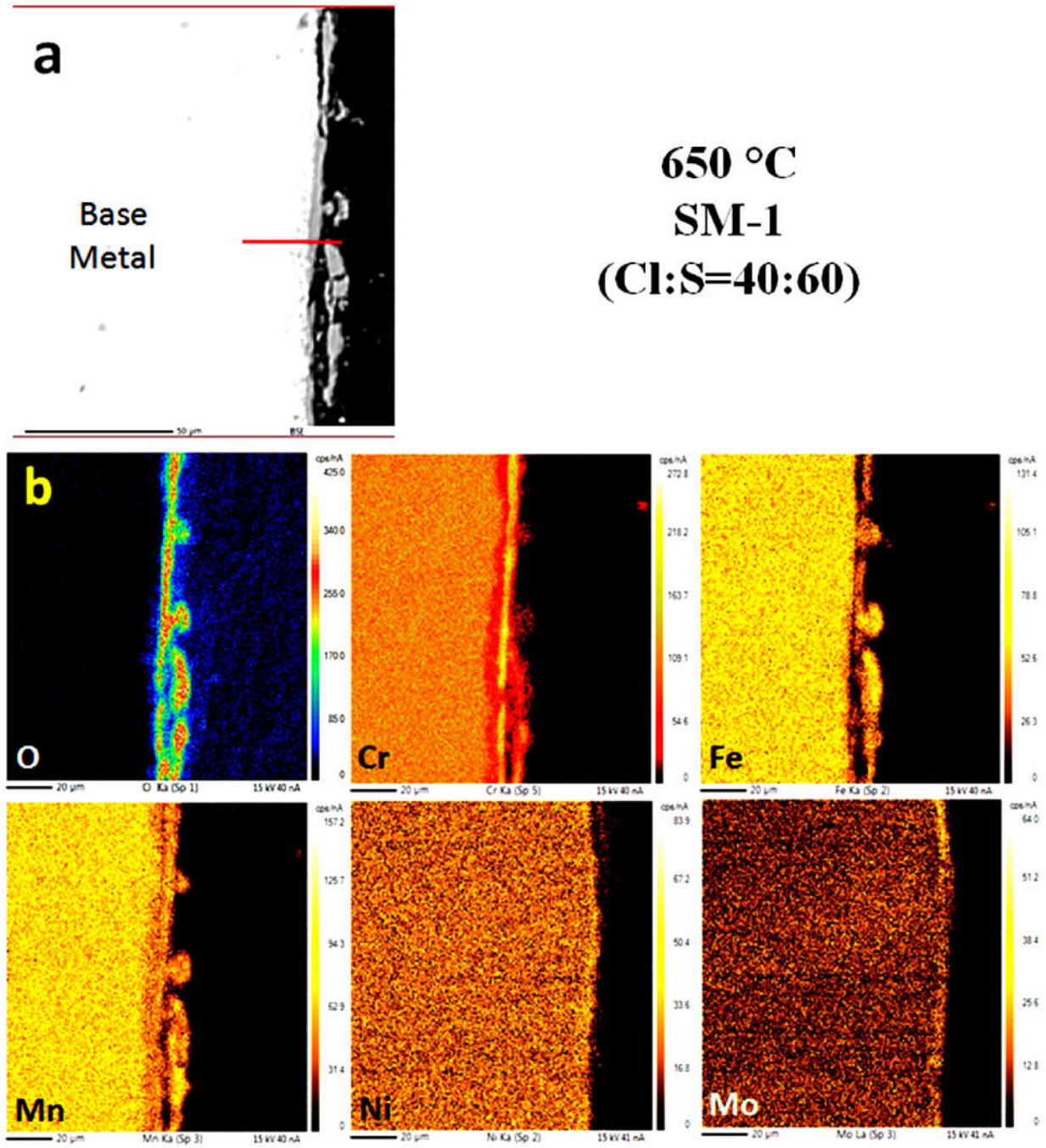

Figure 5.12: EPMA mapping of cross section of the sample hot corroded by SM1 at 650 °C, up to 100 h.

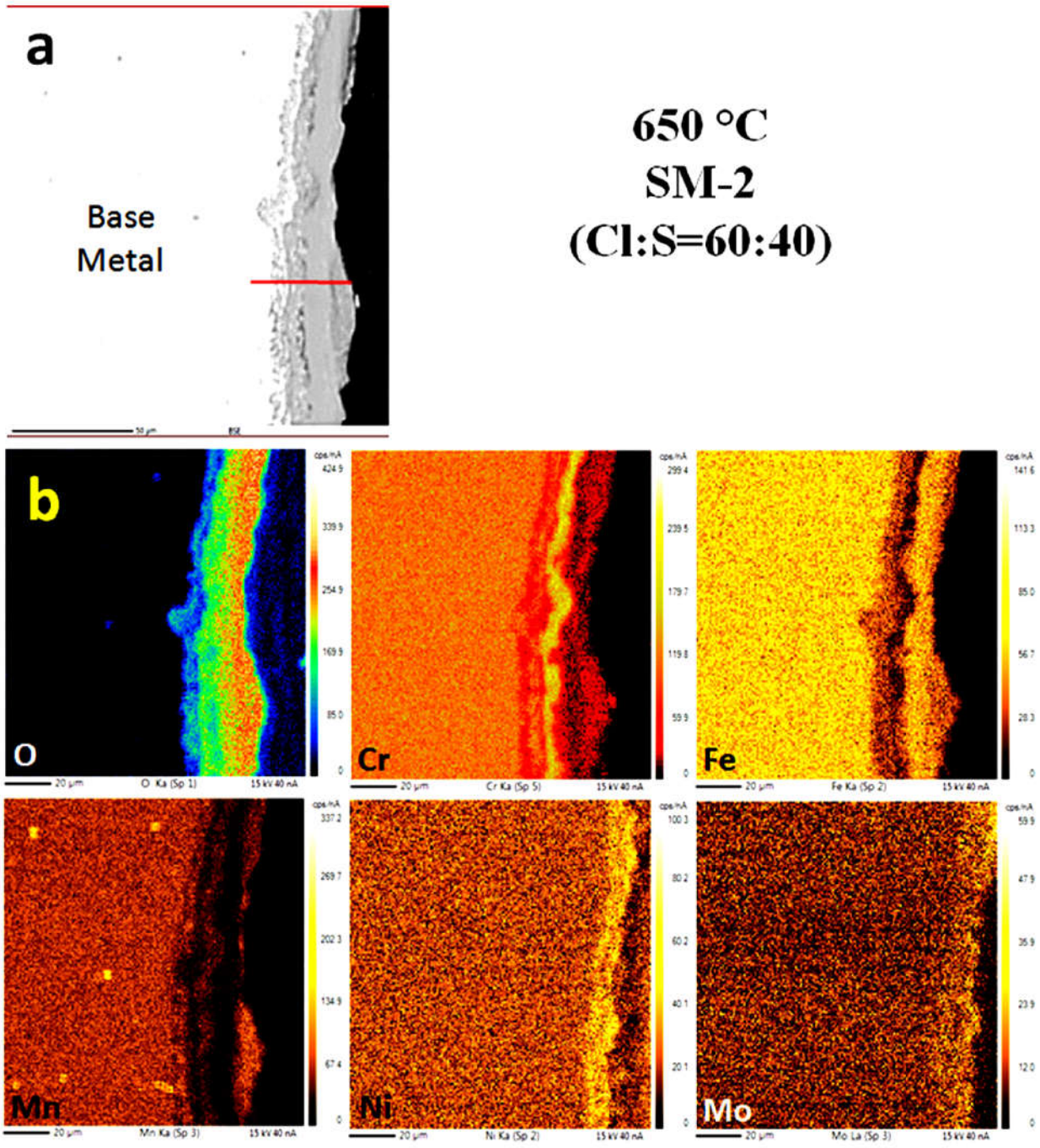

Figure 5.13: EPMA mapping of cross section of sample hot corroded by SM2 salt mixture and exposed at 650 °C up to 100 h.

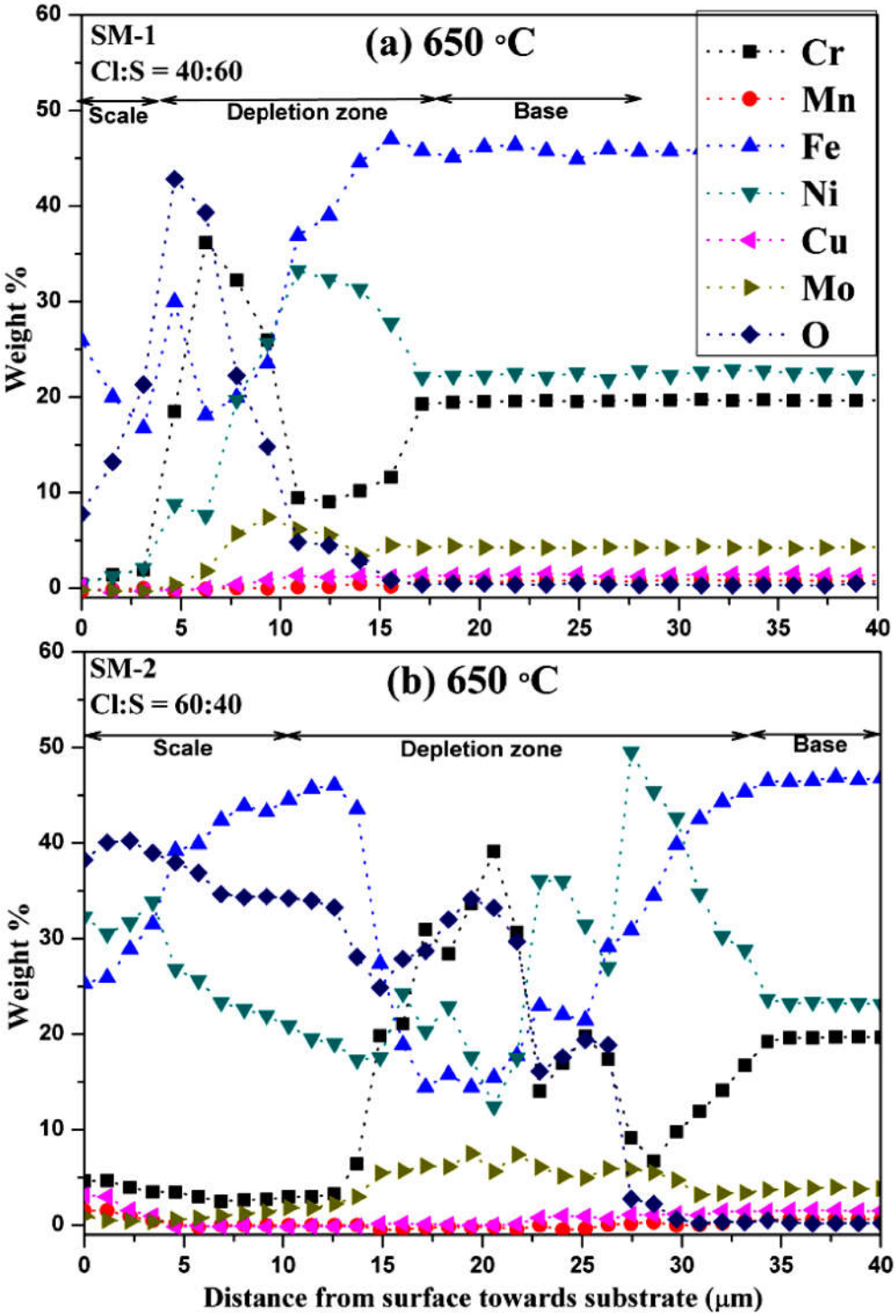

Figure 5.14: EPMA line scans of cross sections of the samples showing variation in concentration of the elements Fe, Ni, Mn, Mo, Cu and O, exposed at 650 °C for 100 h in air, coated with (a) SM1 and (b) SM2.

Table 5.4: Melting temperatures of different salts and eutectic temperatures of different salt mixtures.

Melting Temperature	°C	*Metal salt eutectic*	°C
$CrCl_3$	1150	NaCl-$CrCl_3$	544-593
$NiCl_2$	1030	NaCl-$CrCl_2$	437
$CrCl_2$	820	NaCl-$FeCl_2$	370-374
$FeCl_3$	303	NaCl-$FeCl_3$	151
$FeCl_2$	676	NaCl-Na_2CrO_4	557
Fe_2O_3	1594	KCl-K_2CrO_4	500-700
NaCl	801	$FeCl_2$+$FeCl_3$	606
Na_2SO_4	884	$FeCl_2$+NaCl	372
KCl	771	$FeCl_2$+$NiCl_2$	665
K_2SO_4	1069	$FeCl_3$+$NiCl_2$	456
K_2CrO_4	980	KCl+K_2SO_4	713
		NaCl+Na_2SO_4	617
		KCl+$NiCl_2$	508
		KCl-$FeCl_2$	345
		KCl-NaCl	652

Table 5.5: Depth of attack on the samples coated with salt mixtures SM1 and SM2 exposed at 650 ˚C, up to 100 h.

	Scale (µm)	**Depletion zone (µm)**	**Total Thickness (µm)**
SM1	4-5	11-13	16-18
SM2	10-12	18-20	31-33

5.3. DISCUSSION

The two salt mixtures SM1 and SM2 were selected in such a way that the content of alkali metals (K, Na) remain in equal quantity whereas Cl and S are in the ratios of 40:60 and 60:40 to simulate the biomass ash deposition in waste to energy boilers. The NaCl, KCl, K_2SO_4 and Na_2SO_4 salts form varying eutectic melts which can affect the corrosion

resistance of the material (**Table-5.3**). The effects of the two salt mixtures (SM1 and SM2) are analysed in detail to bring out the influence of alkali high sulphur in presence of chloride salts (Cl:S=40:60) and that of alkali high chlorine in the presence of sulphate salts (Cl:S=60:40). Passivation of a highly corrosion resistant material demands dense microstructure, high adhesion of the protective oxides to substrate and absence of inter-connected pores in them which otherwise serve as preferred diffusion path for the corrosive agents [93].

5.3.1 EFFECT OF ALKALI SALTS WITH HIGH SULPHUR IN PRESENCE OF CHLORINE SALTS (SM1)

It may be seen from **Figure 2** that there was little weight gain from the exposure at 500 ºC due to non fusion of the coated salt mixtures, in agreement with the earlier observation made by Daniel et al [81]. At 550 also there is weight change, more or less with similar trend of linear increase, however, it was relatively more in the sample coated with SM2 (**Figure 2b**). At 600 and 650 °C there was rapid increase in the weight gain from 5-25 h, beyond which the gained weight increased very slowly whereas it increased progressively at 500 and 550 ºC. Since there was no melting of the salt mixtures at 500 °C, the XRD phase analysis showed formation of *in-situ* oxides and in parallel the *ex-situ* diffusion [94] of salt showed less severe corrosive nature of oxides. The much lower value of k_p corresponding to exposure of the samples coated with SM1 and SM2, from 25-100 h may be attributed to decrease in the amount of corrodents due to their high reactivity/instability (**Table 5.6**) and formation of protective layer over the spalled surface region. On the other hand at lower temperature of 500 and 550 ºC the reactivity of corrodents is much less and

their stability is higher, hence a single slope behavior is exhibited (**Figure 5.3**). The much higher level of the $(\Delta W)^2$ vs time plot in **Figure 3b** at 650 °C, as compared to that at 600 °C, may be understood from the difference in the hot corrosion rate which is nearly 15 times higher at 650 °C than that at 600 °C, during 5-25 h of exposure (**Table 5.1**).

The reactions occurring under this condition are shown in **Table 5.3**. During the initial 5 h of exposure there is much less increase in the weight as seen from the inserts, beyond 5 h there is rapid increase in the weight gain only up to 25 h of exposure, and parabolic behavior is exhibited (**Figure 5.3(a-b)**).

It is well known that alkali chlorides accelerate the process of corrosion [40], while the alkali sulphates lower the effects of alkali chlorides in biomass combustion [95]. The cross section of the sample coated with SM1 and exposed at 500 ºC did not show any porous layer because of insufficient melting of the salts.

The scale formed was intact and there was no spallation. On exposure at 550 °C the non-protective feature of the oxide scale may be observed from its porous nature [87]. The difference in surface of the samples corroded with salt mixtures at 550 ºC from that at 500 ºC is due to more penetration of salt mixture into base material at 550ºC. From the weight change at 600 ºC it is seen that weight gain was due to formation of chromia layer as per the reactions between $(Cr,Fe)_2O_3$ matrix and the molten salts (**Table 5.3**). A new species formed at 600 °C with SM1 was Cr_2MnO_4, in agreement with the minimum amount of Mn depleting with chromia layer [96].

In particular at 600 and 650 ˚C (**Figure 5.2 and 5.3**), this behavior reflects rapid growth of oxides induced by chlorination and subsequent rapid oxidation by the process of the so called active oxidation. Presence of $FeCr_2O_4$, Cr_2O_3 on the exposed surface indicates rapid

formation of oxides which is in line with the previous observation made on Sanicro-28 [29]. The cross section of the sample following 100 h of exposure at 600 °C shows that the formed scale tended to separate out from the base metal. This kind of scale layer was also observed at 650 °C, causing separation of scale from the base material due to mechanical stresses induced during cyclic corrosion. At 650 °C there was faster rate of corrosion with higher weight gain resulting from the formation of porous and non-protective layer. From phase analysis it is confirmed that this nature is due to the corrosives such as $K_2Cr_2O_7$ and $Na_2Cr_2O_7$. The above two eutectic mixtures enhanced the rate of corrosion very rapidly.

5.3.2 EFFECT OF ALKALI HIGH CHLORINE IN PRESENCE OF SULPHUR SALTS (SM2)

SEM-EDS analysis of cross section of the sample (**Figure 5.11**) shows that at 650 °C a significant amount of oxides and corrosion products got embedded beneath the scale. These oxides were loosely bonded and spalled. The growth of the other oxides can be seen clearly from the surface morphology (**Figures 5.8** and **5.9**).

The surface morphology of the samples corroded with salt mixture SM2 in the temperature range 500-650 °C, clearly reveals variation in the size of oxides. There is far less spallation from exposure at 500-550 °C whereas it is much higher at 600 ˚C and highest at 650 ˚C in agreement with the observation of Grabke [97] where high alloy steel was found spalled as well as there was porous scale of Fe_2O_3 at the oxide interface due to high chloride content and escape of high volatile chlorides. The high chlorine content in the salt mixture and penetration of Cl^- into the scale resulted in formation of $NiCl_2$, $FeCl_2$, $FeCl_3$ and $CrCl_3$. The inward diffusion of Cl^- ions and outward diffusion of alloying

elements resulted in formation of a thick depleted zone at the interface between the substrate and the scale. These phases in this zone were characterized by the XRD and SEM-EDS analysis and found to be due to chlorides. These chlorides continuously evaporated and iron chloride got oxidized to Fe_3O_4 in air on the top at outer surface of the scale. Thus, it can be called active oxidation of Fe_2O_3 in the presence of chlorine which acts as catalyst and accelerates the process of corrosion at 600-650 °C forming cracks/splat boundaries, grain boundary grooving or fissuring. The outward diffusion of $FeCl_2(g)$ through $Fe_2O_3(s)$ gave rise to an inverse proportion to thickness of the oxide. Effect of SO_2 in the atmosphere on the active oxidation beneath the deposits was in the form of CrS. A modest increase of oxidation rate was observed with high Cl-content rather than S-content. From the literature also, it is clear that sulphur minimizes the effect of chlorine attack from 500-650 °C up to 100 h in air atmosphere [98, 99].

The results obtained by XRD/SEM-EDS and EPMA, clearly indicate that at 500 and 550 °C oxide scale remained almost similar in the two regions and spinel formed. There was formation of spinel which comprises mainly of the M_2O_3 and M_3O_4 oxides, where, M is the transition element such as Fe, Cr, Ni, Mn, Mo and Cu. From **Figures 5.5** and **5.6(a-b)** the amount of corrosives evaluated from EDS analysis confirmed the presence of the phases such as $FeCl_3$, FeS and CrS. Moreover, the potassium salts oxides are $K_2Cr_2O_7$, K_2FeO_4 and $KCrO_2$ and the sodium based oxides $NaCrO_2$, $Na_2Cr_2O_7$ and $NaFeO_2$ were found from the EDS analysis. With increase in temperature of the sample coated with SM1 to 600 °C and 650 °C, there was no change in potassium products while in the sample with SM2 coating $K_2Cr_2O_7$ got converted to K_2CrO_4 and $Na_2Cr_2O_7$ to Na_2CrO_4 respectively [100-102].

EPMA analysis of the cross section and the line scans of the samples exposed at 650 °C show that there was a significant outward diffusion of Fe and Ni from the base metal to the scale. A thick crust of oxides rich in Fe and Ni can be seen in **Figure 5.13**. It is also important to note that at lower temperatures of 500-550 °C the alloy surface showed pits and uneven interface, whereas at the higher temperatures of 600-650 °C the surface of the sample was uniformly eaten away by the corrodents and a layered structure formed comprising of several laminar cracks.

5.3.3 CORROSION MECHANISM

5.3.3.1 SIGNIFICANCE OF ALKALI METALS, CHLORIDES AND SULPHATES

Presence of the both, alkali chlorides as well as sulphates was detected near/over the external oxide-internal oxide interface in both the samples coated with SM1 as well as SM2, exposed at 550, 600 and 650 °C. The interfaces of these formed oxides were selectively attacked by the salt mixtures while they were absent near the matrix. Again, it should be noted that due to volatile nature of the salts of Na, K, Cl, S (established by the EDS analysis) their concentration at the scale surface was found to be in lower proportion and was negligible near the internal oxides at the substrate. This site is called corrosion front [103]. Thus, it also means that depleted layer below the corrosion front consisted of Cl, S rather than Na and K. This reaction proceeded in such a way that oxides were first dissociated/broken by chlorine and then chlorine proceeded towards attacking the internal oxides. Potassium and sodium were not found to proceed/propagate below the corrosion front. This phenomena or process of attack by chlorine rather by Na, S, K was reported by Yohaness et al. [82], Li et al. [41] and Peterson et al. [85]. The chromium and iron were

depleted from the surface and consumed by K and Na, whereas chlorine and sulphur associated with Ni and Fe formed $NiCl_2$, $FeCl_2$, FeS, NiS and made the reaction proceed towards the depleted zone.

5.3.3.2 CORRELATION OF EPMA ANALYSIS WITH FREE ENERGY DATA

It is clear from the EPMA analysis that chromium and iron played major role in prevention of the protective layer. The colour contrast of each individual element shows that the scale formed from the exposure at 650 °C with SM1 and SM2 clearly reveals that iron oxides converted in the form of $FeCl_2$, FeS and chromium oxides in the form of $CrCl_2/CrCl_3$, CrS, have been all over the surface region. In the case of corrosive oxides at the surface scale, it is also revealed that, iron and chromium oxide ($(Cr,Fe)_2O_3$) reacted with K and Na and formed low melting eutectics with (Na,K)-Fe-O and (Na,K)-Cr-O over the scale.

As shown in the **Table. 5.6**, ΔG values were calculated by standard free energy equation for the phases formed during the process of corrosion. Among all the ΔG values presented for the different oxides, it is evident that Cr_2O_3 is the most stable and formed rapidly in the process of corrosion at any temperature. In case of the chlorides, $CrCl_2/CrCl_3$, KCl and NaCl, were found to be more stable from 500-650 ˚C and the most unstable phase was $MnCl_2$. In the case of sulphur compounds, FeS(α) has the highest tendency of formation among the sulphides and has higher melting point. It is important to understand that the volatilization of chlorides and sulphates played important role in the process of corrosion. Also, from the **Table 5.6** it can be observed that Fe-Cl system has low stability than that of FeS system and is highly volatile and due to high vapour pressure its inward and outward movement has been highly effective in generation of porous layer.

Focusing on the values of ΔG for KCl and NaCl, it should be noted that the values at 500-650 ˚C are almost comparable [104]. Another important observation in the present investigation is that the ratio of Na:K is same and there is difference only in the ratio of Cl:S. From the **Tables 5.4** and **5.6** and EPMA analysis it can be summarized that in the formation of scale at the chromium, iron and oxygen play the important role. Below the corrosion front it can be seen that the content of iron, chromium, nickel oxides as well as their chlorides/sulphates are highly stable at 500 ˚C, while they are unstable at 650 ˚C. The observed results are in line with the reactions of corrosion with high content of chlorine than sulphur.

Table 5.6: Calculated values of Gibbs free energy (kJ/mole) for the different phases resulting from corrosion by SM1 and SM2 from 100 h of exposure at 500-650 ˚C.

ΔG (in kJ/mole)	**Fe_2O_3**	**Fe_3O_4**	**Cr_2O_3**	**$FeCr_2O_4$**	**NiO**	**$FeCl_2$ (α)**	**$FeCl_3$**	**$CrCl_2$**
ΔG_{500}	-140.7	-215.5	-919.4	-472.3	-168.5	-247.1	-16.8	-296.3
ΔG_{550}	-133.7	-209.3	-906.4	-467.3	-164.2	-241.3	-24.9	-290.8
ΔG_{600}	-126.6	-203.0	-893.4	-462.2	-159.9	-235.6	-33.0	-285.4
ΔG_{650}	-119.6	-196.7	-880.4	-457.2	-155.7	-229.9	-41.1	-280.1
ΔG (in kJ/mole)	**$CrCl_3$**	**FeS (γ)**	**MnS (α)**	**MnO**	**$MnCl_2$ (α)**	**K_2O**	**KCl(s)**	**NaCl(s)**
ΔG_{500}	-246.1	-219.4	-218.2	-77.4	-383.7	-261.1	-361.3	-337.9
ΔG_{550}	-239.1	-214.1	-215.0	-73.8	-377.8	-254.9	-356.3	-333.0
ΔG_{600}	-232.1	-208.8	-211.8	-70.1	-372.0	-248.8	-351.2	-328.0
ΔG_{650}	-225.1	-203.4	-208.6	-66.5	-366.2	-242.8	-346.2	-323.1

5.4. CONCLUSION

1. Hot corrosion from both the salt mixtures SM1 and SM2 was quite slow during the initial exposure of 5 h at 500-650 ˚C. However, it increased rapidly during 5-25 h but reduced drastically from 25-100 h and dual slope was observed.
2. Hot corrosion at the lower temperature of 550 ˚C, and particularly at 500 ˚C, from both SM1 and SM2 was much less and slower over the period of exposure from 5-100 h.
3. The salt mixture SM2 with high ratio of Cl:S=60:40 caused much severe hot corrosion at 550-650 ˚C in comparison with that of SM1 with Cl:S=40:60.
4. The high rate of corrosion due to SM1 and SM2 at 600 and 650 ˚C was from active oxidation due to penetration of Cl^- ions in the scale and formation of chlorides.